Capacitive charge storage at an electrified interface investigated via direct first-principles simulations

Maxwell D. Radin, Tadashi Ogitsu, Juergen Biener, Minoru Otani, and Brandon C. Wood

Phys. Rev. B **91**, 125415 — Published 11 March 2015

DOI: 10.1103/PhysRevB.91.125415

Capacitive charge storage at an electrified interface via direct first-principles simulations

Maxwell D. Radin

*Department of Physics, University of Michigan, Ann Arbor, MI 48105**

Tadashi Ogitsu, Juergen Biener, and Brandon C. Wood†

Materials Science Division, Lawrence Livermore National Laboratory, Livermore, CA 94550

Minoru Otani

National Institute of Advanced Industrial Science and Technology, Tsukuba, Japan

Abstract

Understanding the impact of interfacial electric fields on electronic structure is crucial to improving the performance of materials in applications based on charged interfaces. Supercapacitors store energy directly in the strong interfacial field between a solid electrode and a liquid electrolyte; however, the complex interplay between the two is often poorly understood, particularly for emerging low-dimensional electrode materials that possess unconventional electronic structure. Typical descriptions tend to neglect the specific electrode-electrolyte interaction, approximating the intrinsic "quantum capacitance" of the electrode in terms of a fixed electronic density of states. Instead, we introduce a more accurate first-principles approach for directly simulating charge storage in model capacitors using the Effective Screening Medium method, which implicitly accounts for the presence of the interfacial electric field. Applying this approach to graphene supercapacitor electrodes, we find that results differ significantly from the predictions of fixed-band models, leading to improved consistency with experimentally reported capacitive behavior. The differences are traced to two key factors: the inhomogeneous distribution of stored charge due to poor electronic screening, and interfacial contributions from the specific interaction with the electrolyte. Our results are used to revise the conventional definition of quantum capacitance and to provide general strategies for improving electrochemical charge storage, particularly in graphene and similar low-dimensional materials.

PACS numbers: 31.15.E-, 82.47.Uv, 73.22.Pr, 82.45.Mp

I. INTRODUCTION

Interfacial electric fields play a critical role in a wide variety of energy storage applications. Supercapacitors represent one important example, since they store charge via the creation of an "electrical double layer" (EDL) at the interface with the electrode as the ionic electrolyte solution responds dynamically to charge accumulation or depletion.[1] Currently, there is great interest in replacing conventional electrode materials with emerging low-dimensional alternatives that promise higher supercapacitor energy densities;[2–10] however, the capacity of these materials is often severely limited by the number of electronic states available for charge storage in the solid-state electrode (sometimes called the quantum capacitance).[11–15] Understanding the relationship between an electrode's electronic structure and the observed capacitance in the presence of an interfacial electric field is therefore essential for predicting and optimizing the performance of next-generation supercapacitors and other electrochemical devices.

In practice, the presence of the EDL induces a strong electric field ($\sim 10^9$ V/m) at the electrode-electrolyte interface, which alters the charge distribution within the electrode and creates a space-charge layer. For conventional metallic electrodes, efficient screening minimizes the impact of this redistribution; however, this is often not the case for systems derived from graphene and similar low-dimensional materials, where screening tends to be poor due to a low electronic density of states (DOS). Most prior theoretical studies[14,16,17] have tended to rely upon the fixed-band approximation (FBA), in which electrode charging or discharging shifts the overall Fermi level as bands fill or deplete. However, the FBA neglects the effect of the interfacial field and instead assumes a homogenous distribution of net charge carriers.

In this paper, we introduce a new model for simulating capacitive charging from first principles, from which the quantum capacitance can be directly extracted. Our approach relies on the effective screening medium (ESM) method[18] to go beyond the FBA and explicitly account for the effects of the EDL-induced interfacial electric field, more closely approximating conditions experienced during device operation. We apply our approach to graphene electrodes to demonstrate that charge redistribution at the interface significantly impacts the observed quantum capacitance and is the likely origin of critical discrepancies[16,17,19] between calculated and measured capacitances. The nature of these variations provides valuable in-

sights for understanding the fundamental effects of the EDL on electrode behavior and for tuning capacitance in real devices.

II. QUANTUM CAPACITANCE BEYOND THE FIXED-BAND APPROXIMATION

The capacitance associated with the electrode-electrolyte interface can be thought of as two capacitances in series, one associated with the liquid electrolyte and the second with the solid electrode (i.e., split by a Gibbs dividing surface). While the accumulation of charge in the first is determined by ion concentration and thermal reorganization, in the second it is typically limited by quantum effects, i.e., the "quantum" capacitance. Formally, the area-specific differential quantum capacitance is given by

$$C_{\mathrm{q}} = \frac{\mathrm{d}\sigma}{\mathrm{d}V_{\mathrm{q}}}, \tag{1}$$

where σ is the surface charge density on the electrode and $V_q = -\mu/e$ measures the chemical potential of electrons μ relative to the energy of an electron at the electrostatic potential of the dividing surface (plus an arbitrary constant). Here e is the elementary charge. The quantum capacitance of graphene electrodes has conventionally been estimated via the FBA:[14,16,17]

$$C_{\mathrm{q}}^{\mathrm{FBA}} = e^2 n(\mu^{\mathrm{FBA}}, N_0). \tag{2}$$

We use the notation $n(E, N)$ to refer to the areal electronic density of states (DOS) at energy E when the system has a total of $N = N_0 - \sigma/e$ electrons per unit area. Neglecting thermal effects, the electron chemical potential $\mu(N)$ is defined implicitly according to:

$$\int_{-\infty}^{\mu(N)} n(E, N)\,\mathrm{d}E = N. \tag{3}$$

Within the FBA, $n(E, N) \approx n(E, N_0)$, and $\mu^{\mathrm{FBA}}(N)$ is instead determined by

$$\int_{-\infty}^{\mu^{\mathrm{FBA}}(N)} n(E, N_0)\,\mathrm{d}E = N. \tag{4}$$

However, in principle it is necessary to account for the accumulation of excess charge near surfaces in accordance with Gauss' law. This requires a more general relation for the quantum capacitance in terms of the DOS. Consider what happens when an infinitesimal

amount of electrons ΔN are added. The new chemical potential $\mu(N+\Delta N)$ is given by

$$\int_{-\infty}^{\mu(N+\Delta N)} n(E, N+\Delta N)\,\mathrm{d}E = N + \Delta N. \tag{5}$$

Splitting the integral yields two terms:

$$\begin{aligned} &\int_{-\infty}^{\mu(N)} n(E, N+\Delta N)\,\mathrm{d}E \\ &+ \int_{\mu(N)}^{\mu(N+\Delta N)} n(E, N+\Delta N)\,\mathrm{d}E \\ &= N + \Delta N. \end{aligned} \tag{6}$$

Expanding the first term on the left-hand side of Eq. 6 to first order in ΔN yields

$$\begin{aligned} &\int_{-\infty}^{\mu(N)} n(E, N+\Delta N)\,\mathrm{d}E \\ &= \int_{-\infty}^{\mu(N)} \left\{ n(E, N) + \frac{\delta n(E, N)}{\delta N}\Delta N \right\} \mathrm{d}E \\ &= N + \Delta N \int_{-\infty}^{\mu(N)} \frac{\delta n(E, N)}{\delta N}\Delta N\,\mathrm{d}E, \end{aligned} \tag{7}$$

where $\delta n(E, N)/\delta n$ is the functional derivative of the DOS with respect to the number of electrons in the system. Similarly, the second term on the left-hand side of Eq. 6 can be expanded as

$$\int_{\mu(N)}^{\mu(N+\Delta N)} n(E, N+\Delta N)\,\mathrm{d}E = \frac{\mathrm{d}\mu}{\mathrm{d}N} n(E, N)\Delta N. \tag{8}$$

The quantum capacitance in Eq. 1 can be alternatively formulated as

$$C_\mathrm{q} = e^2 \frac{\mathrm{d}N}{\mathrm{d}\mu}. \tag{9}$$

Inserting Eqs. 7 and 8 into Eq. 6 and solving for C_q according to the definition in Eq. 9 yields the more general expression

$$C_\mathrm{q} = e^2 \frac{n(\mu, N)}{1 - \int_{-\infty}^{\mu(N)} \frac{\delta n(E,N)}{\delta N}\,\mathrm{d}E}. \tag{10}$$

Note that although the Kohn-Sham eigenvalues are not rigorously equivalent to the actual excitation energies, Janak's theorem[20] implies that the density of Kohn-Sham eigenvalues obeys Eq. 3. Therefore, the above derivation still applies regardless of whether $n(E, N)$ represents the density of excitation energies or the density of Kohn-Sham eigenvalues.

We point out that Eq. 10 reduces to the FBA when $\int_{-\infty}^{\mu(N)} \frac{\delta n(E,N)}{\delta N}\,\mathrm{d}E$ is small (i.e., when the DOS is unaffected by excess charge) or when ΔN is small (i.e., there is little excess charge on

the electrode). In the later sections, we will show that in the case of graphene electrodes, the FBA provides an incomplete quantitative description once we consider electronic screening limitations and charge redistribution in the presence of the EDL.

III. COMPUTATIONAL DETAILS

ESM calculations were performed within a plane-wave pseudopotential density functional theory (DFT) formalism using the van der Waals density functional (vdW-DF)[21–23] with a revised Perdew-Burke-Ernzerhof (revPBE) exchange reference,[24,25] as implemented in Quantum Espresso.[26] Full geometry optimizations were done using a $24 \times 24 \times 1$ k-point mesh within the primitive cell, and forces were converged to within 10^{-5} Ry/Bohr. A finer k-point grid of $96 \times 96 \times 1$ was used for the capacitance calculations, with a 0.1 eV electronic smearing. A vacuum spacing of > 9 Å separated periodic images.

Additional Born-Oppenheimer molecular dynamics simulations of a graphene-water interface were performed, with the ESM method applied with three charge states: neutral, $+0.005e$ per carbon atom ($+0.27e$ for the simulation cell), and $-0.005e$ per carbon atom ($-0.27e$ for the simulation cell). The latter cases correspond roughly to -0.25 V and $+0.25$ V, based on integration of the carbon density of states.[15] Simulations consisted of 54 carbon atoms in a hexagonal ($3\sqrt{3} \times 3\sqrt{3}$) unit cell with 54 water molecules. Because we were interested only in the atomic structure of the interface rather than electronic energies, we used gamma-only k-point sampling. The cell size perpendicular to the graphene basal plane was 13Å, sufficient to allow for some vacuum separation between the cell edge and the water at the end farthest from the graphene electrode. The cell temperature was maintained at 400 K using a velocity rescaling approach. The initial configuration was determined by first equilibrating bulk water independently for 5 ps, then placing it in contact with the graphene at an initial separation of 3 Å. The system was then re-equilibrated for 1 ps at neutral charge before enabling the voltage bias. The dynamics were then run for an additional 0.5 ps before collecting production data over a 3 ps interval.

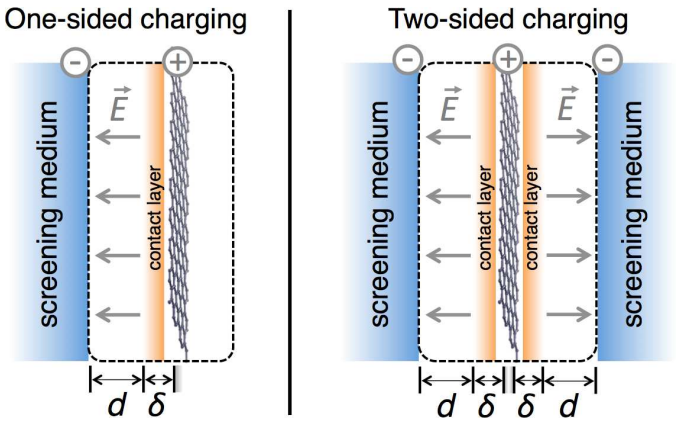

FIG. 1. (Color online) Simulation setup for one- and two-sided charging within the ESM method (shown here for positive bias).

IV. SIMULATION SETUP

In this paper, we outline a methodology for directly computing the response of V_{q} to σ within the ESM framework,[18] which yields a more realistic view of charge and discharge that is fully compatible with Eq. 10. The ESM method inserts an infinite-dielectric medium at the boundary of the periodic simulation cell. Buildup of a mirror charge within this medium generates an interfacial electric field as the electrode is charged or discharged, mimicking the actual response of a supercapacitor electrode in contact with an ideal-screening "perfect" electrolyte.

The electrode capacitance was determined within two distinct configurations, shown schematically in Fig. 1. In the first (Fig. 1a), a perfect-screening medium was placed parallel to the surface at one of the cell edges; this configuration mimics an electrode with one side in contact with an electrolyte (one-sided charging). In the second (Fig. 1b), two perfect-screening media were placed at opposite cell edges, which mimics an electrode with both sides in contact with an electrolyte (two-sided charging). These two representative configurations were chosen to span a variety of device setups and materials.[2–6,27]

One could compute the quantum capacitance by placing the cell boundary at the position of the dividing surface, which lies a distance δ from the surface nuclei. However, this would require a different set of DFT calculations to be performed for different positions of the dividing surface. Instead, we place the cell boundary a fixed distance away from the slab and map the system on to an equivalent circuit of two series capacitances: one associated with

the differential quantum capacitance of the electrode C_{q}, and the other with the capacitance C_{v} due to the potential drop across the vacuum between the dividing surface and screening medium:[13]

$$\frac{1}{C} = \frac{1}{C_{\mathrm{q}}} + \frac{1}{C_{\mathrm{v}}} \tag{11}$$

For two-sided charging, the last term on the right-hand side of Eq. 11 is doubled because there are contributions from two gap regions. The total capacitance of the simulation cell C was determined by numerically differentiating the σ-V relationship obtained from a series of single-point calculations at different values of σ. V was calculated as the Fermi level relative to the energy of a free electron at the electrostatic potential in the screening region(s). We model C_{v} in Eq. 11 as a parallel plate capacitor, $C_{\mathrm{v}} = \varepsilon_0/d$, where d is the distance from the dividing surface to the screening medium. The voltage drop V_{q} associated with the electrode is given by

$$V_{\mathrm{q}}(\sigma) - V_{\mathrm{q}}(0) = \int_0^Q \frac{1}{C_{\mathrm{q}}(\sigma')}\,\mathrm{d}\sigma', \tag{12}$$

where $V_{\mathrm{q}}(0)$ corresponds to the potential of zero charge.

The value of δ is in principle arbitrary and reflects the partitioning of the voltage drop between the electrode and electrolyte. However, it is convenient to choose the position of the Gibbs dividing surface as the position where the screening of electric fields by the electrolyte begins; then the quantum capacitance represents the capacitance that would be measured if the electrolyte were a perfect screening medium. Thus we envision δ as representing the inner boundary of the electrolyte (see Fig. 1). For now, we adopt the van der Waals radius ($\delta = r_{\mathrm{w}} = 1.70$ Å for carbon[28]); this choice is motivated by the fact that the van der Waals radius gives a good description of cavities in continuum solvation models, as it represents the approximate distance to electrons in an electrolyte.[29] We will return a detailed discussion of the significance of δ later.

V. QUANTUM CAPACITANCE OF GRAPHENE

To illustrate the importance of the additional considerations within the ESM-based simulation of capacitive charging, we apply our approach to single-layered (SLG) and multi-layered graphene electrodes, which are known to exhibit particularly severe quantum capacitance limitations.[11–16] The corresponding differential quantum capacitance profiles are shown in Fig. 2 (note that reported capacitances are normalized with respect to electrolyte

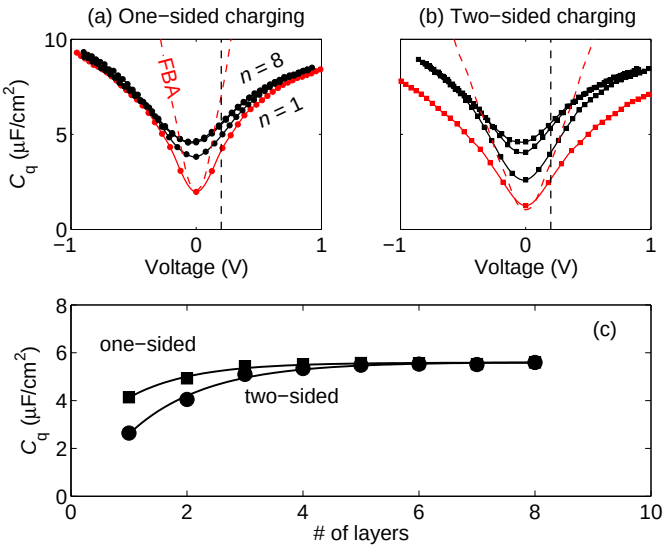

FIG. 2. (Color online) Dependence of calculated area-specific differential quantum capacitance on the number of graphene layers n for (a) one-sided and (b) two-sided charging, for slabs 1 (red), 2, 4 and 8 layers thick. The dashed red line shows the FBA-derived capacitance. (c) Comparison of values at a bias of +0.2 V (dashed vertical line in (a) and (b)). The solid lines show a fit to an exponential form.

contact area; i.e., two-sided charging has twice the surface area of one-sided charging). We initially focus our discussion on SLG (red curves). The minimum in the capacitance corresponds to the Dirac point, at which the zero-temperature DOS for SLG is in principle zero; here, although we have used a very fine k-point grid, the additional electronic smearing used in the DFT calculations results in a non-zero DOS. Corrections for this effect are explored further below.

It is immediately evident from Fig. 2 that the slope of the capacitance with voltage predicted by our direct simulation method (based on $\delta = 1.70$ Å) is much shallower than that predicted by the FBA (dashed line). Thus, the presence of the interfacial electric field reduces the effective capacitance of the graphene electrode. By contrast, a recent DFT study by Paek *et al.* suggested that polarization does not significantly affect the quantum capacitance of graphene, based on the observation that the presence of an ionic-liquid electrolyte had little impact on the DOS of uncharged graphene within the FBA. Note that this conclusion is restricted to regimes where the FBA applies. As Fig. 2 demonstrates, the FBA does not apply to the full range of potentials relevant for practical devices, and so in general,

calculations not accounting for interfacial electric fields and the concomitant polarization effects may not be representative of real graphitic electrodes. This highlights the advantages of considering the implicit relationship in Eq. 10 within our direct charging simulation framework. We point out that Paek *et al.* did report significant charge redistribution and a strong effect on the double-layer capacitance component; in our model, a portion of these effects are instead included in C_{q} based on our choice for the dividing surface (between graphene and the electrolyte, rather than on the graphene atomic layer).

Experimental measurements of the quantum capacitance of single-layer graphene[16,17,19,32,33] exhibit considerable variability in magnitude, due in large part to different reported values for the minimum capacitance. For example, estimates of the capacitance at a bias of +0.2 V relative to the potential of minimum capacitance range from ∼2 to ∼10 $\mu\mathrm{F/cm^2}$.[16,17] Differences in the capacitance minimum may be attributed to artifacts of the specific model used to extract or compute C_{q}, as well as systematic contributions from the substrate or other components in the cell that are amplified at small capacitance values. However, the slope of the quantum capacitance with voltage in the quasi-linear regime provides a more robust measure for comparison that does not directly depend on the absolute value of minimum capacitance.

Figure 3 compares various experimental measurements of C_{q} derived from electrochemical or field-effect transistor setups where interface polarization plays a role.[16,17,19] Compared to fixed-band models (dashed lines), the results universally demonstrate a shallower-than-expected capacitance dependence, as has been pointed out by the authors of those studies (we have aligned all capacitance minima to allow easier comparison). On the other hand, agreement with our direct charge/discharge simulations is quite reasonable. Note that because the electronic smearing used in our ESM calculations is physically equivalent to an elevated electron temperature, it may not be appropriate to compare directly with room-temperature experiments. Accordingly, we have also included in Fig. 3 an estimate of C_{q} at room temperature, based on temperature-scaling our ESM results according to models of idealized graphene:[31]

$$C_{\mathrm{q}}(T) \propto T \ln\left[2\left(1+\cosh\frac{eV}{\mathrm{k_B}T}\right)\right]. \tag{13}$$

In certain cases, the temperature scaling improves the agreement even further. The largest deviations from our calculated results are found in the measurements of Chen and Appenzeller,[17] which show an unusually shallow capacitance that is even further from

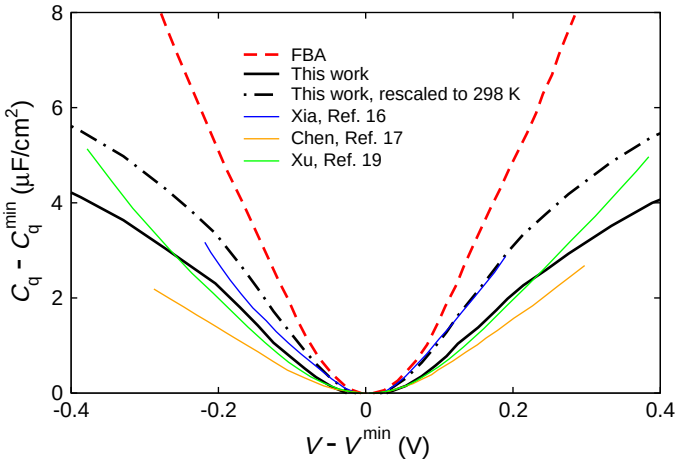

FIG. 3. (Color online) Comparison between measured quantum capacitance of single-layer graphene (thin lines, from Refs. 16, 17, and 19) and our ESM-derived predictions for one-sided charging (thick black solid and dashed-dotted lines are unscaled and temperature-rescaled via Eq. 13, respectively). The corresponding FBA result is shown as a dashed red line. Voltages and capacitance values are referenced to the minima in the capacitance curves ($V^{\min}$ and $C_{\rm q}^{\min}$).

the FBA. However, the authors also state that the high AC voltage they use will tend to underestimate $C_{\rm q}$ by a factor of two; accounting for this factor brings the results in excellent agreement with our predictions.

Notably, impurities[16] or local potential fluctuations[19] within the graphene plane have been invoked to reconcile the measured deviations from the behavior expected from the FBA or a two-dimensional electron gas model. These inhomogeneities—attributed to the presence of dopants, defects, substrates, or charge puddling—alter local carrier concentrations and affect the quantum capacitance.[15,16,19] Instead, our findings suggest that these same patterns are *intrinsic* to freestanding pristine graphene once the effect of the interfacial electric field is taken into account. Specifically, we hypothesize that local potential fluctuations are induced by field-induced charge inhomogeneity normal to the electrode surface. Our data may also help to explain why Fermi velocities of graphene (proportional to the inverse slope of the dependence in Fig. 3) tend to be higher when obtained from best-fit models in electrochemical or field-effect transistor setups—where interfacial fields are present—compared to direct measurements by other methods.[16,19,34,35]

Charge redistribution influences the relative capacitances of one- and two-sided charging of SLG. The FBA assumes that any such charge redistribution is negligible, which leads

to a one-sided capacitance that is double that of two-sided after normalizing by the electrolyte contact area. In contrast, the ratio of the ESM capacitance of SLG for one-sided charging to that of two-sided charging is $1.2 - 1.6$ over the voltage range considered (see Fig. 2). The difference can be attributed to the redistribution of excess charge towards the side of the graphene facing the EDL, an effect not accounted for in the FBA. Accordingly, space-charge limitations become even more critical in the presence of the EDL; this effect certainly contributes to the anomalously low area-specific capacitance observed in high-surface area carbon electrodes[2,11] as the screening length approaches the pore wall thickness.[13] The space-charge limitation is explored further in the dependence of the capacitance on the electrode thickness in Fig. 2, defined as the number of layers n of graphitic AB slabs. As the thickness increases, space-charge screening limitations become less severe. Accordingly, the capacitances for both one- and two-sided charging increase and ultimately converge. The magnitude of the space-charge effect is voltage dependent, and is most evident at potentials near the capacitance minimum, where the DOS is lowest (the notable exception is SLG under two-sided charging, which exhibits the largest space-charge effect of all). For instance, at $+0.2$ V (Fig. 2c), we find that for one-sided charging, the capacitance plateaus at $\sim$3 layers, beyond which the electric field is fully screened. For two-sided charging, slightly thicker slabs ($\sim$5 layers) are required to reach the maximum capacitance because both sides of the electrode must now screen the field. The curves in Fig. 2c follow an exponential form, and can be fit to $C_{\mathrm{q}}(n) = C_{\infty} - \Delta C \exp\left[-\kappa(n-1)\right]$ in order to estimate a characteristic length κ^{-1} of 1.1 and 1.3 layers for one- and two-sided charging, respectively ($\sim$1.8 and 2.2 Å). This length is related to the distance at which charge redistribution is no longer limiting the capacitance, and reflect our prior analysis of the Debye screening length in graphitic slabs based only on polarization effects.[15]

A close inspection of Figs. 2a and 2b shows that in addition to an increase in capacitance with the number of layers, there is also a small shift in the position of the minimum towards lower potentials. The potential of minimum capacitance decreases by $\sim$20 mV as the number of layers goes from one to eight. This is consistent with the fact that in graphite, the Fermi level lies not at the minimum of the DOS, but slightly below the minimum.[36] It also agrees with electrochemical experiments that have found the potential of minimum capacitance of glassy carbon to be $\sim$20 mV lower than that of an activated carbon aerogel, whose building blocks are closer to SLG.[12]

Next, we return to a discussion of our chosen definition for δ. Recent studies have reported a region of low electron density between the electrode and the Stern layer of the electrolyte.[37,38] Ando *et al.* termed this region the "contact layer", which they showed exists due to Pauli repulsion at the interface (in the absence of specific adsorption).[37] Here, we associate the contact layer with the electrode capacitance, and therefore include it in our definition of δ (see Fig. 1); however, we emphasize that in reality, it is a purely interfacial characteristic that derives from the interaction between the electrode and the electrolyte.

The low electron density in the contact layer leads to poor screening and a concomitant voltage drop that profoundly influences the capacitance. The sensitivity of the calculated capacitance to δ is shown in Fig. 4, with the effects most pronounced at high voltage magnitudes and for small values of δ. To interpret this result, consider that physically, the contact layer thickness is related to the approach distance of the electrolyte to the electrode, and more particularly to the distance at which the electronic density associated with the electrolyte atoms becomes appreciable. This distance can depend on several factors, including the interaction strength between the electrode and electrolyte (e.g., surface hydrophobicity or hydrophilicity), as well as the voltage. Accordingly, Fig. 4 asserts that the identity of the electrolyte could have a significant effect on the interfacial capacitance of the electrode, even in the limit of a short Debye length in the liquid. This finding is directly analogous to the recent discovery of strong capacitance changes due to the formation of a low-dielectric interface in nanoscale capacitors, also revealed by first-principles calculations.[39]

In addition, local variations in the electrolyte approach distance will broaden our single value for δ into a distribution of values. This effect is explored in Fig. 4c, which shows the probability distribution of closest approach distances of electrolyte atoms in short first-principles molecular dynamics simulations of a graphene-water interface at 0, -0.25, and $+0.25$ V, computed within the ESM framework (using a one-sided charging configuration). The broadening in our calculated distributions is indeed nonnegligible (width at half maximum $\sim$1.0 Å); this will enhance the average capacitance because the sensitivity to δ is higher at shorter approach distances (Fig. 4b). (Note that the approach distance is based on the atomic positions rather than electron density, and hence is systematically larger than δ.) The distributions also skew and shift with applied bias. The magnitudes of these shifts are of the order of $+0.4$ AA for positive bias and -0.2 Å for negative bias. Interestingly, this means the contact layer effect on capacitance should be asymmetric with voltage. It

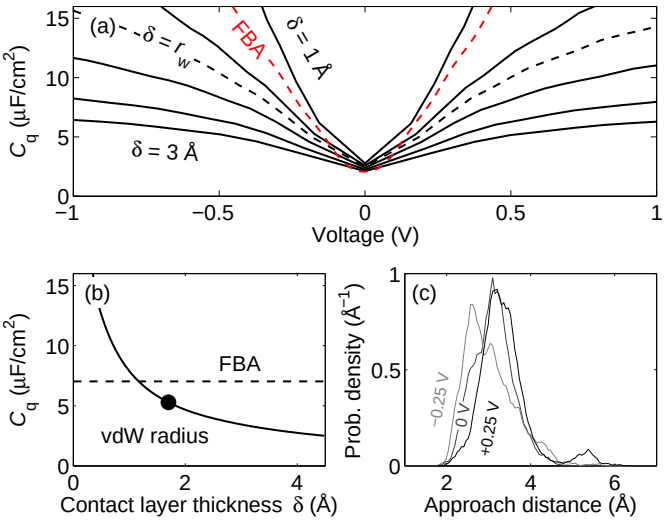

FIG. 4. (Color online) (a) Calculated differential quantum capacitance as a function of voltage for δ going from 1 to 3 Å in increments of 0.5 Å (solid lines). Results based on the carbon van der Waals radius (r_w) are also shown. The red dashed line shows the FBA-derived capacitance. (b) Calculated differential quantum capacitance for the two-sided charging of SLG at a bias of +0.2 V as a function of contact layer thickness δ. The maximum value of δ considered, 4.5 Å, corresponds to half of the simulation cell length. The black circle shows the capacitance for δ equal to the carbon van der Waals radius, and the horizontal dashed line shows the FBA-derived capacitance. (c) Average approach distance from a graphene electrode to the closest liquid atom in first-principles dynamics simulations of a water-graphene interface at 0 V, +0.25 V, and −0.25 V.

also leads us to conclude that not only does the average electrolyte approach distance impact the interfacial capacitance of the electrode, but so does the *distribution* of approach distances. This introduces the possibility of using the properties of the electrolyte to tune the electrode capacitance, and suggests that different electrolyte compositions or additives could have significantly different effects.[40–42] An alternative approach may be to use confinement geometries to alter the approach distance distribution.[43] Understanding these effects in terms of specific electrolyte compositions represents a promising future research direction.

VI. CONCLUSIONS

In summary, we outline an approach for directly simulating capacitive charging in the presence of an interfacial electric field derived from the electrical double layer. We show that

for systems with intrinsic screening limitations (i.e., low-dimensional electrodes), accounting for space-charge effects and interfacial interactions in the presence of this field is critical for properly describing charge storage. These effects, which are missing in conventional fixed-band descriptions, are the origin of significant systematic errors in the computed capacitance of graphene. Based on our findings, the observed capacitance of the electrode depends on the choice of electrolyte because the latter couples to the electrode capacitance through the interfacial contact layer. Our results point to two avenues for tuning the quantum capacitance in supercapacitors and similar electrochemical devices. The first is to address the screening within the electrode by increasing the thickness or modifying the dielectric properties. The second is to engineer the electrolyte to tune its interaction with the electrode and modify the approach distance distribution. We suggest that this could be done with the a proper choice of electrolyte or additive, or by leveraging confinement effects. We point out that the approach presented here is general, and may be broadly applied to understand interfacial charge storage across a wide variety of electrochemical systems.

ACKNOWLEDGMENTS

This work was performed under the auspices of the U.S. Department of Energy under by LLNL under Contract DE-AC52-07NA27344. Funding was provided by Laboratory Directed Research and Development Program Grant 12-ERD-035, with computing support from the LLNL Institutional Computing Grand Challenge Program. The authors acknowledge helpful discussions with M. Merrill and J. R. I. Lee.

---

* Present address: Materials Department, University of California, Santa Barbara, CA 93106

† brandonwood@llnl.gov

[1] A. Burke, J. Power Sources **91**, 37 (2000).

[2] J. Biener, M. Stadermann, M. Suss, M. A. Worsley, M. M. Biener, K. A. Rose, and T. F. Baumann, Energy Environ. Sci. **4**, 656 (2011).

[3] E. Frackowiak, Phys. Chem. Chem. Phys. **9**, 1774 (2007).

[4] Y. Zhai, Y. Dou, D. Zhao, P. F. Fulvio, R. T. Mayes, and S. Dai, Adv. Mater. **23**, 4828 (2011).

[5] A. G. Pandolfo and A. F. Hollenkamp, J. Power Sources **157**, 11 (2006).

[6] D.-W. Wang, F. Li, M. Liu, G. Q. Lu, and H.-M. Cheng, Angew. Chem. Int. Ed. **47**, 373 (2008).

[7] J. M. Soon and K. P. Loh, Electrochem. Solid-State Lett. **10**, A250 (2007).

[8] J. Feng, X. Sun, C. Wu, L. Peng, C. Lin, S. Hu, J. Yang, and Y. Xie, J. Am. Chem. Soc. **133**, 17832 (2011).

[9] S. Ratha and C. S. Rout, ACS Appl. Mater. Interfaces **5**, 11427 (2013).

[10] M. D. Stoller, S. Park, Y. Zhu, J. An, and R. Ruoff, Nano Lett. **8**, 3498 (2008).

[11] O. Barbieri, M. Hahn, A. Herzog, and R. Kötz, Carbon **43**, 1303 (2005).

[12] L.-H. Shao, J. Biener, D. Kramer, R. N. Viswanath, T. F. Baumann, A. V. Hamza, and J. Weissmüller, Phys. Chem. Chem. Phys. **12**, 7580 (2010).

[13] H. Gerischer, J. Phys. Chem. **89**, 4249 (1985).

[14] M. D. Stoller, C. W. Magnuson, Y. Zhu, S. Murali, J. W. Suk, R. Piner, and R. S. Ruoff, Energy Environ. Sci. **4**, 4685 (2011).

[15] B. C. Wood, T. Ogitsu, M. Otani, and J. Biener, J. Phys. Chem. C **118**, 4 (2014).

[16] J. Xia, F. Chen, J. Li, and N. Tao, Nat. Nanotechnol. **4**, 505 (2009).

[17] Z. Chen and J. Appenzeller, 2008 IEEE Int. Electron Devices Meet., 1 (2008).

[18] M. Otani and O. Sugino, Phys. Rev. B **73**, 115407 (2006).

[19] H. Xu, Z. Zhang, and L.-M. Peng, Appl. Phys. Lett. **98**, 133122 (2011).

[20] J. F. Janak, Phys. Rev. B **18**, 7165 (1978).

[21] M. Dion, H. Rydberg, E. Schröder, D. C. Langreth, and B. I. Lundqvist, Phys. Rev. Lett. **92**, 246401 (2004).

[22] T. Thonhauser, V. R. Cooper, S. Li, A. Puzder, P. Hyldgaard, and D. C. Langreth, Phys. Rev. B **76**, 125112 (2007).

[23] G. Román-Pérez and J. M. Soler, Phys. Rev. Lett. **103**, 096102 (2009).

[24] J. P. Perdew, K. Burke, and M. Ernzerhof, Phys. Rev. Lett. **77**, 3865 (1996).

[25] Y. Zhang and W. Yang, Phys. Rev. Lett. **80**, 890 (1998).

[26] P. Giannozzi *et al.*, J. Phys. Condens. Matter **21**, 395502 (2009).

[27] Y. Sun, Q. Wu, and G. Shi, Energy Environ. Sci. **4**, 1113 (2011).

[28] A. Bondi, J. Phys. Chem. **68**, 441 (1964).

[29] J. Tomasi, B. Mennucci, and R. Cammi, Chem. Rev. **105**, 2999 (2005).

[30] E. Paek, A. J. Pak, and G. S. Hwang, J. Chem. Phys. **142**, 024701 (2015).

[31] T. Fang, A. Konar, H. Xing, and D. Jena, Appl. Phys. Lett. **91**, 092109 (2007).

[32] F. Giannazzo, S. Sonde, V. Raineri, and E. Rimini, Nano Lett. **9**, 23 (2009).

[33] S. Dröscher, P. Roulleau, F. Molitor, P. Studerus, C. Stampfer, K. Ensslin, and T. Ihn, Appl. Phys. Lett. **96**, 152104 (2010).

[34] R. Gillen and J. Robertson, Phys. Rev. B **82**, 125406 (2010).

[35] L. A. Ponomarenko, R. Yang, R. V. Gorbachev, P. Blake, A. S. Mayorov, K. S. Novoselov, M. I. Katsnelson, and A. K. Geim, Phys. Rev. Lett. **105**, 136801 (2010).

[36] J. McClure, Phys. Rev. **108**, 612 (1957).

[37] Y. Ando, Y. Gohda, and S. Tsuneyuki, Chem. Phys. Lett. **556**, 9 (2013).

[38] G. Cicero, J. C. Grossman, E. Schwegler, F. Gygi, and G. Galli, J. Am. Chem. Soc. **130**, 1871 (2008).

[39] M. Stengel and N. A. Spaldin, Nature **443**, 679 (2006).

[40] M. Galiński, A. Lewandowski, and I. Stępniak, Electrochim. Acta **51**, 5567 (2006).

[41] M. Armand, F. Endres, D. R. MacFarlane, H. Ohno, and B. Scrosati, Nature Mater. **8**, 621 (2009).

[42] P. Jungwirth and D. J. Tobias, Chem. Rev. **106**, 1259 (2006).

[43] J. Chmiola, G. Yushin, Y. Gogotsi, C. Portet, P. Simon, and P. L. Taberna, Science **313**, 1760 (2006).